SPANDIDOS PUBLICATIONS

ONCOLOGY REPORTS 46: 220, 2021

# Ultrasound-targeted microbubble destruction-mediated overexpression of Sirtuin 3 inhibits the progression of ovarian cancer

LI CHENG*, DONGMEI ZHANG* and WEI YAN

Department of Electrical Diagnosis, Affiliated Hospital of Changchun University of Traditional Chinese Medicine, Changchun, Jilin 130021, P.R. China

Received June 19, 2019; Accepted November 26, 2020

DOI: 10.3892/or.2021.8171

**Abstract.** Ultrasound-targeted microbubble destruction (UTMD) has recently been developed as a promising noninvasive tool for organ- and tissue-specific gene or drug delivery. The aim of the present study was to explore the role of UTMD-mediated Sirtuin 3 (SIRT3) overexpression in the malignant behaviors of human ovarian cancer (HOC) cells. Reverse transcription-quantitative PCR was performed to detect *SIRT3* mRNA expression levels in normal human ovarian epithelial cells and HOC cell lines; low *SIRT3* expression was found in HOC cell lines, and the SKOV3 cell line was used in the following experiments. The *SIRT3*-microbubble (MB) was prepared, and the effects of ultrasound-treated *SIRT3*-MB on biological processes of SKOV3 cells were determined. The proliferation, migration, invasion and apoptosis of SKOV3 cells were measured after *SIRT3* upregulation by UTMD. Xenograft tumors in nude mice were induced to observe tumor growth *in vivo*. Upregulation of *SIRT3* inhibited the malignant behaviors of SKOV3 cells, whereas UTMD-mediated *SIRT3* upregulation further inhibited proliferation, epithelial-mesenchymal transition, invasion and migration, and induced apoptosis of SKOV3 cells, and it also inhibited tumor formation and growth *in vivo*. Moreover, the present study identified hypoxia inducible factor-1α (HIF-1α) as a target of *SIRT3*. The present study provided evidence that UTMD-mediated overexpression of *SIRT3* may suppress HOC progression through the inhibition of HIF-1α.

*Correspondence to:* Ms. Li Cheng, Department of Electrical Diagnosis, Affiliated Hospital of Changchun University of Traditional Chinese Medicine, 1478 Gongnong Road, Changchun, Jilin 130021, P.R. China
E-mail: chengli_33339@163.com

*Contributed equally

*Key words:* ovarian cancer, Sirtuin 3, ultrasound-targeted microbubble destruction, epithelial-mesenchymal transition, apoptosis, hypoxia inducible factor-1α

## Introduction

Human ovarian cancer (HOC) is a major life-threatening gynecological malignancy that accounts for ~3% of all cancer incidences in females, with 240,000 newly diagnosed cases and 150,000 deaths from HOC annually worldwide (1). Owing to the absence of early symptoms, HOC is usually diagnosed at advanced stages that are difficult to cure by simple surgical resection, and relapse commonly occurs during the clinical course of HOC (2). Most patients with HOC exhibit peritoneal metastases and suffer from perennial malignant ascites leading to advanced stages, a massive progression and poor prognosis of HOC (3,4). Despite surgical interventions and the administration of anticancer drug combinations, the 5-year survival rate of patients with advanced-stage HOC remains low (5); owing to the distinct biology of HOC, the effective treatment for this disease remains limited (1). Thus, it is urgent to develop novel and more effective treatments for this disease.

A previous study revealed that several members of the sirtuin (SIRT) family (*SIRT1-SIRT7*), the mammalian homologues of the yeast silent information regulator (*Sir2*) gene, serve crucial roles in the development of cancers (6). The SIRT family includes a specific class of nicotinamide adenine dinucleotide ($NAD^+$)-dependent deacetylase that targets several protein substrates to carry out diverse biological functions, such as oxidative stress regulation, metabolism, cell survival, division and aging (6,7). SIRT3 is expressed as a full-length 44-kD protein that is targeted to the mitochondria by its N-terminal localization sequence, and it uniquely regulates apoptosis and cell survival; it functions either as a tumor promoter or inhibitor depending on the cell or tumor type and on the different types of stress or cell apoptosis stimuli (8). *SIRT3* is expressed at low levels in human breast cancer and lung cancer (9), acting as a genomically expressed, mitochondrial-located tumor suppressor (10,11). Similarly, aberrant low expression of *SIRT3* was demonstrated in patients with gastric cancer (12). *SIRT3* was also indicated to be downregulated in prostate carcinoma, and *SIRT3* overexpression inhibited prostate cancer cell proliferation and improved patient survival (13). The current study delivered the *SIRT3* gene with ultrasound-targeted microbubble destruction (UTMD). UTMD has emerged as a novel gene therapy that appears to be safe and repeatable, enables

the plasmids in the bubbles to avoid degradation in blood, and avoids safety issues of previous gene delivery systems and focuses on gene delivery to target tissues (14-16). UTMD has been documented to enhance tissue or cell penetration and to serve as a supportive technique for cancer therapies (17,18). The current study assessed the biological mechanisms of the *SIRT3* gene delivered by UTMD in the malignant behavior of HOC cells to provide a theoretical foundation for a novel target treatment for HOC.

## Materials and methods

*Cell culture*. The HOC cell lines COC1, A2780 and SKOV3 and the normal human ovarian epithelial cell line HOSEpiC were purchased from National Collection of Authenticated Cell Cultures of The Chinese Academy of Sciences and incubated in cell culture dishes at a density of $1x10^5$ cells/$cm^2$. The cells were cultured in RPMI-1640 medium (COC1 and SKOV3), DMEM (A2780) or minimum essential medium (MEM; HOSEpiC) (all purchased from Gibco; Thermo Fisher Scientific, Inc.) supplemented with 10% FBS (Hyclone; Cytiva) at 37˚C with 5% $CO_2$ for 48 h. When confluence reached 80-90%, cells were detached with 0.025% trypsin (Gibco; Thermo Fisher Scientific, Inc.) and passaged.

*SIRT3 recombinant vector construction*. The lentiviral vector pLVX-IRES-ZsGreen1, which contains the green fluorescent protein (GFP) reporter gene, was purchased from Clontech Laboratories, Inc. Human SIRT3 cDNA was synthesized by Shanghai Sangon Biotech Co., Ltd. A *SIRT3* target cDNA fragment was ligated into pLVX-IRES-ZsGreen1 vector to generate pLVX-*SIRT3*-IRES-ZsGreen1 overexpression vector (*SIRT3* vector).

*Microbubble (MB) preparation*. Cationic lipid MBs were synthesized using polyethylene glycol-40 stearate (1 mg/ml), 1-distearoyl phosphatidylcholine (2 mg/ml), 1,2-dicarboxyl-3-trifluoromethyl propane (0.4 mg/ml) and decafluorobutane gas (all purchased from Avanti Polar Lipids, Inc.) by ultrasonic dispersion (220 V, 50 Hz, 100 W for 20 sec, at an interval of 10 sec; 10 cycles in total) in aqueous phase. The MBs were observed under an optical microscope (x400 magnification), and the particle size and electric potential were measured using a Malvern Zetasizer Nano ZS90 (Malvern Instruments, Inc.). The *SIRT3* vector (4.0 $\mu$g) was incubated in 50 $\mu$l MB suspension at 37˚C for 30 min. The plasmids that did not bind to the MBs were washed out with PBS. The *SIRT3*-loaded MB was obtained and was resuspended in 500 $\mu$l RPMI-1640 medium for subsequent experiments.

*Cell transfection and grouping*. Exponentially growing SKOV3 cells ($1x10^5$ cells/ml) at passage 3 were seeded into 6-well plates, and 50 $\mu$l *SIRT3*-MB suspension was added to each well, followed by 1 MHz ultrasound treatment for 30 min at 2.5 W/$cm^2$; these cells were designated the *SIRT3*-MB group. The ultrasonic therapeutic apparatus was provided by Institute of Ultrasound Imaging of Chongqing Medical University (Chongqing, China) (19). In addition, 4.0 $\mu$g *SIRT3* vector or empty vector was mixed with 2 $\mu$l Lipofectamine® 2000 (Invitrogen; Thermo Fisher Scientific, Inc.) and further resuspended in 500 $\mu$l RPMI-1640 medium; 50 $\mu$l *SIRT3* suspensions or empty vector suspensions were loaded onto 6-well plates and named the *SIRT3* group or the negative control (NC) group, respectively. Moreover, SKOV3 cells mixed with 500 $\mu$l RPMI-1640 medium were used as the blank group. At 24 h post transfection, GFP in cells was observed under an Olympus FSX100 fluorescence microscope (x100 magnification; Olympus Corporation), and the mRNA and protein expression levels of SIRT3 in cells was measured using reverse transcription-quantitative PCR (RT-qPCR) and western blot analysis, respectively, to validate the transfection efficiency.

*RT-qPCR*. Total RNA from $5x10^7$ HOC cells was extracted using the TRIzol® (Invitrogen; Thermo Fisher Scientific, Inc.) one-step method, and the RNA quality was identified by formaldehyde denaturing gel electrophoresis. cDNA was generated by RNA reverse transcriptase M-MLV (cat. no. RP1105, Beijing Solarbio Science & Technology Co., Inc.); the reaction conditions were as follows: 42˚C for 60 min, and 95˚C for 5 min. SYBR Green (Takara Biotechnology Co., Ltd.) was used to conduct qPCR, and PCR primers (Table I) were designed and synthesized by Shanghai Sangon Biotech Co., Ltd., with β-actin set as the internal reference. The PCR volume was 15 $\mu$l, and the reaction conditions were as follows: Initial denaturation at 96˚C for 5 min; followed by 30 cycles of denaturation at 94˚C for 40 sec, annealing at 53˚C for 45 sec and extension at 72˚C for 1 min; and a final extension at 72˚C for 10 min. The PCR product was examined using agarose gel electrophoresis to test the length and concentration of the amplified fragment (data not shown). Data were analyzed using the $2^{-\Delta\Delta Cq}$ method (20), where Cq is the quantitation cycle and $2^{-\Delta\Delta Cq}$ refers to the ratio of the target gene expression between the experimental group and the control group. The formula is as follows: $\Delta\Delta Cq=[Cq\ (\text{target gene})-Cq\ (\text{control gene})]_{\text{experiment group}}-[Cq\ (\text{target gene})-Cq\ (\text{control gene})]_{\text{control group}}$.

*Western blot analysis*. When the confluence of HOC cell lines reached about 70%, the cells were treated for 48 h with MB or recombinant plasmid, and then protein was extracted using RIPA lysis buffer (cat. no. P0013B; Beyotime Institute of Biotechnology), and protein concentration was determined in accordance with the instructions of the BCA kit (Qiagen GmbH). Extracted proteins (20-40 $\mu$g) were separated by 12% SDS-PAGE at a voltage from 80 to 120 V, and subsequently transferred onto PVDF membranes using a semidry method (at 80 mV for 30-45 min). The membranes were blocked with 5% BSA (cat. no. AR0185; Boster Biological Technology) for 1 h at room temperature and subsequently incubated at 4˚C overnight with primary antibodies (all from Abcam) against the following antigens: Cleaved caspase-3 (1:1,000; cat. no. ab2302), pro-caspase 3 (1:10,000; cat. no. ab32499), Bcl-2 (1:1,000; cat. no. ab32124), cleaved caspase-9 (1:500; ab2324), pro-caspase 9 (1:1,000; cat. no. ab138412), hypoxia inducible factor-1α (HIF-1α; 1:500; cat. no. ab51608), Vimentin (1:1,000; cat. no. ab193555), E-cadherin (1:50; cat. no. ab1416), N-cadherin (1:100; cat. no. ab18203) and β-actin (1:5,000; cat. no. ab227387). Following three washes (5 min each) with TBS + 0.05% Tween-20 (TBST), membranes were incubated with a horseradish peroxidase (HRP)-labeled goat anti-rabbit

Table I. Primer sequences used for reverse transcription-quantitative PCR.

| Gene | Primer sequence (5'→3') |
|---|---|
| *SIRT* | F: CCGCTCGAGATGGCGTTCTGGGGTTGG |
| *SIRT* | R: CGCGGATCCCTATTTGTCTGGTCCATCA |
| E-cadherin | F: TCACATCCTACACTGCCCAG |
| E-cadherin | R: AGTGTCCCTGTTCCAGTAGC |
| N-cadherin | F: AGGGGACCTTTTCCTCAAGA |
| N-cadherin | R: TCAAATGAAACCGGGCTATC |
| Vimentin | F: GGACCAGCTAACCAACGACA |
| Vimentin | R: AAGGTCAAGACGTGCCAGAG |
| HIF-1α | F: TCCAGAAGGAGTTCTTATTCG |
| HIF-1α | R: AAAATCTCATCCAAGAAGCC |
| β-actin | F: ACAGTCAGCCGCATCTTCTT |
| β-actin | R: GACAAGCTTCCCGTTCTCAG |

F, forward; R, reverse; HIF-1α, hypoxia inducible factor-1α; SIRT3, Sirtuin 3.

IgG (H + L) secondary antibody (1:1,000; cat. no. A0208; Beyotime Institute of Biotechnology) at room temperature for 1 h and washed with TBST three times (5 min each) before chemiluminescence development using BeyoECL Plus (cat. no. P0018S; Beyotime Institute of Biotechnology). A Bio-Rad Gel Doc EZ Imager (Bio-Rad Laboratories, Inc.) was used to visualize the protein bands. The signal intensity of target bands was analyzed using ImageJ software V1.8.0 [National Institutes of Health (NIH)]. β-actin was used to normalized protein expression levels.

*Transwell invasion assay*. The top chamber of each 24-well Transwell was precoated with Matrigel (BD Biosciences) for 30 min, filled with 30 $\mu$l RPMI-1640 medium and placed in a $CO_2$ incubator. The SKOV3 cells were detached using trypsin, centrifuged at 800 x g for 3 min at room temperature, and then resuspended using serum-free RPMI-1640 medium and dispersed into a cell suspension at a density of $5x10^5$ cells/ml. The lower chamber was filled with 500 $\mu$l 10% FBS-supplemented RPMI-1640 medium and loaded with 200 $\mu$l cell suspension. The cells were cultured at 37˚C with 5% $CO_2$ for 48 h. Subsequently, the medium in the chambers was washed with PBS, and the cells were stained with 0.1% crystal violet for 10 min at room temperature. Excess crystal violet was washed away with running water, and cells on the upper membrane were removed with a cotton swab, images of the cells on the lower membrane were captured under an Olympus X71 inverted phase contrast microscope (magnification, x100; Olympus Corporation) for manual cell number calculation.

*Wound healing assay*. Cell migration was examined using the scratch test. HOC cells were seeded on 6-well plates at $5x10^5$ cells per well and cultured in complete medium with 10% FBS at 37˚C with 5% $CO_2$ for 24 h. When cells reached 90% confluency, a 1 ml pipette tip was used to produce a scratch on the cell monolayer and the cells were washed with PBS and cultured with serum-free medium at 37˚C. Images of the wounds were captured under an Olympus X71 inverted phase contrast microscope (magnification, x100; Olympus Corporation) at 0, 24 and 48 h. ImageJ software V1.8.0 (NIH) was used to analyze and calculate the scratch area. The ratio of scratch area of differently treated cells to scratch area of the same cells at 0 h represented the relative cell migration rate.

*MTT assay*. HOC cells from each group at logarithmic growth phase were detached using trypsin and resuspended to $1x10^4$ cells/ml single cell suspension in RPMI-1640 medium containing 10% FBS-. The suspension was mixed and plated on 96-well plates at 200 $\mu$l ($2x10^3$ cells) per well; wells filled with culture medium and without cells were used as the blank control. Five duplicated wells were set for each group. The cells were cultured in a 37˚C incubator with 5% $CO_2$ for 0-3 days. MTT solution (20 $\mu$l of 5 mg/ml) was added at 0, 24, 48 and 72 h, and the culture was terminated 4 h later with the supernatant of each well discarded. The well was filled with 200 $\mu$l dimethyl sulfoxide to remove the purple formazan crystals, and the plate was vortexed for 10 min to fully dissolve the purple formazan crystals at room temperature. The optical density (OD) value of each well at $OD_{490}$ was detected using multifunctional enzyme label analyzer (Molecular Devices, LLC).

*5-Ethynyl-2'-deoxyuridine (EdU) labeling assay*. Exponentially growing SKOV3 cells at passage 3 were collected, and the DNA replication ability of cells was detected using a Cell-Light EdU Apollo567 In Vitro Kit (Guangzhou RiboBio Co., Ltd.) following the manufacturer's instructions. Five views of cells were randomly selected and observed under a fluorescence microscope (magnification, x100). The blue fluorescence (DAPI) refers to all cells, and the red fluorescence indicates the replicating cells stained by EdU. The EdU-positive cell rate in five randomly selected fields was determined by ImageJ software V1.8.0 (NIH).

*Colony formation assay*. SKOV3 cells in logarithmic growth phase were collected, detached with 0.025% trypsin and seeded on 6-well plates at a density of 1,000 cells/well for incubation at 37˚C with 5% $CO_2$ for 14 days. Subsequently, the cells were fixed with 75% methanol for 30 min at room temperature, followed by staining with 0.2% crystal violet at room temperature. Under an Olympus X71 inverted phase contrast microscope (magnification, x100; Olympus Corporation), 10 fields were randomly selected and the number of clones with >50 cells in the field were counted; each experiment was repeated three times.

*Flow cytometry*. Cell cycle and apoptosis were detected by cell cycle and apoptosis detection kit (cat. no. C1052; Beyotime Institute of Biotechnology). For the cell cycle assay, cells were detached at 37˚C using trypsin into single cells, and the detachment was terminated after adding the serum-contained medium; next, cells were centrifuged at 800 x g at room temperature for 3 min, the supernatant was discarded, and

the pellet was resuspended and washed with PBS to adjust the cell concentration to $1x10^6$ cells/ml. The single cell suspension was centrifuged at 1,000 x g for 5 min at room temperature and the supernatant was discarded. Cells were mixed with 500 $\mu$l 70% cold ethanol and fixed at 4˚C overnight. After discarding the fixation solution, the cells were further washed with 1 ml PBS and centrifuged at 1,000 x g for 3 min at room temperature; the supernatant was discarded. The cells were then treated with 100 $\mu$l RNase A and incubated in a water bath at 37˚C for 30 min. Subsequently, the cells were mixed with 400 $\mu$l propidium iodide (PI) at 4˚C in the dark for 30 min for detection. The red fluorescence at a wavelength of 480 nm was recorded using a flow cytometer (Beckman Coulter, Inc.) and the data were analyzed using CellQuest software v3.3 (BD Biosciences).

For the apoptosis assay, the cell suspension was mixed with 2 $\mu$l Annexin V-FITC (20 $\mu$g/ml) and allowed to stand on ice in the dark for 15 min. Next, the mixture was transferred into the flow cytometry tube and mixed with 300 $\mu$l PBS, after which each sample was further mixed with 1 $\mu$l PI (50 $\mu$g/ml) and detected within 30 min using a flow cytometer (Beckman Coulter, Inc). Modfit software v5.0 (Verity Software House, Inc.) was used for analysis. The results were interpreted as follows: Annexin V-FITC was set as the horizontal axis and PI was set as the vertical axis, with the upper-left quadrant containing the mechanically injured cells, the upper-right quadrant containing the late apoptotic cells or necrotic cells, the lower-left quadrant containing the negative normal cells and the lower-right quadrant containing the early apoptotic cells. Total apoptotic rates were measured as the sum of early- and late-stage apoptosis.

*Xenograft tumors in nude mice*. A total of 40 specific-pathogen-free grade BALB/c nude mice [age, 4-6 weeks; weight, 20±2 g; purchased from Beijing Vital River Laboratory Animal Technology Co., Ltd.; animal license. no. SCXK (Beijing) 2015-0001] were numbered by weight and randomly assigned into four groups (n=10 mice/group). The mice were separately housed at a constant temperature (20±2˚C) and humidity (50-60%) with free access to food and water under a 12-h light-dark cycle. The housing conditions met the requirements for environmental facilities for medical laboratory animals. A total of $4x10^6$ SKOV3 cells were suspended in 200 $\mu$l physiological saline and subcutaneously injected into the nude mice through the right axilla. At 7 days post-injection, the SIRT3 vector or NC empty vector was diluted in 200 $\mu$l saline and then injected into the mice through the caudal vein, and the groups of mice were correspondingly named the SIRT3 group and the NC group. Similarly, the SIRT3-MB vector was diluted in 200 $\mu$l saline and injected into the mice and subjected to 10 min of ultrasound treatment at 10 MHz at the cancer cell transplantation sites; this group was named the SIRT3-MB group. A blank group was set as a control in which nude mice were injected with an equal volume of saline. From the date of transplantation, the behavior (excessive excitement, fighting, abnormal calls or excessive fear), activity, response to external stimulation (human touch, change of light), diet, defecation and weight of nude mice were observed every day to monitor their health and behavior. Tumor formation was also recorded every day. The tumor volume of the mice was measured every 7 days and calculated as follows: (length x width$^2$)/2 for a total of 35 days (21). After subcutaneous injection, each mouse bore only one tumor. On day 35 following cell injection, the tumors were 1-1.5 cm in length, accompanied by weight loss and decreased response to external stimuli (Fig. S1). The mice were then euthanized by intraperitoneal administration of overdose of pentobarbital (800 mg/kg) (22,23). After observation of pupil dilation and complete cardiac arrest, the tumors were removed, weighed and prepared for immunohistochemical assays.

*Immunohistochemical assay*. The extracted mouse tumor tissues of each group were fixed using 4% paraformaldehyde at 4˚C for 24 h, embedded in paraffin, dewaxed and cut into five sections (4 $\mu$m each). The sections were washed three times with PBS, and subsequently incubated with 3 drops of 3% $H_2O_2$ at room temperature for 15 min to eliminate the activity of endogenous peroxidase. After three washes with PBS, the slices were incubated with normal goat serum (cat. no. AR0009; Wuhan Boster Biological Technology, Ltd.) blocking solution and allowed to stand at room temperature for 15 min. Next, the slices were incubated at 4˚C overnight with the following primary antibodies obtained from Abcam (50 $\mu$l each): Anti-Ki67 (1:500; cat. no. ab15580), anti-E-cadherin (1:100; cat. no. ab1416) and anti-N-cadherin (1:100; cat. no. ab18203). The slices were then washed with PBS three times, followed by the incubation with HRP-AffiniPure Goat Anti-Rabbit IgG (H + L) secondary antibodies (1:500; cat. no. 1:500; Wuhan Boster Biological Technology, Ltd.) for 15 min at 37˚C. Following three PBS washes, the tissues were incubated with 40 $\mu$l HRP-labeled streptomyces ovalbumin solution (2 $\mu$g/ml; cat. no. SY0746-CIK; Beijing Biolab Technology Co., Ltd.) in PBS at 37˚C for 15 min. After three PBS washes, the slices were treated with 2,4-diaminobutyric acid (DAB) for color reaction for 3-5 min at room temperature, after which they were washed with distilled water and counterstained with hematoxylin for 30 sec at room temperature, and finally dehydrated using an ascending series of ethanol and sealed with neutral gum. Five non-overlapping fields were randomly selected for each slice and observed under an LED5000 light microscope (magnification, x100; Leica Microsystems GmbH). The number of positive cells was counted.

*Dual luciferase reporter assay*. HIF-1α is a possible target gene of SIRT3 (24). The mutant-type (MT) sequence and wild-type (WT) sequence of the binding sites of HIF-1α and SIRT3 were designed. The MT sequence and WT sequence fragments were cloned into the pmir-GLO vector (Promega Corporation). The pmir-GLO vector containing the MT sequence was co-transfected with SIRT3 vector or empty vector NC into SKOV3 cells using the Lipofectamine® 3000 (Invitrogen; Thermo Fisher Scientific, Inc.) which were subsequently named the MT + SIRT3 group and the MT + NC group, respectively. Likewise, the pmir-GLO vector containing the WT sequence was transfected in similar combinations, and the groups were named the WT + SIRT3 group and the WT + NC group. The fluorescence intensity of cells in each group was measured with a Dual Luciferase Reporter Gene Detection kit (Beijing Yuanpinghao Biotech Co., Ltd.) 48 h after transfections using a GloMax 20/20 luminometer (Promega Corporation). *Renilla* activity was used for normalization.

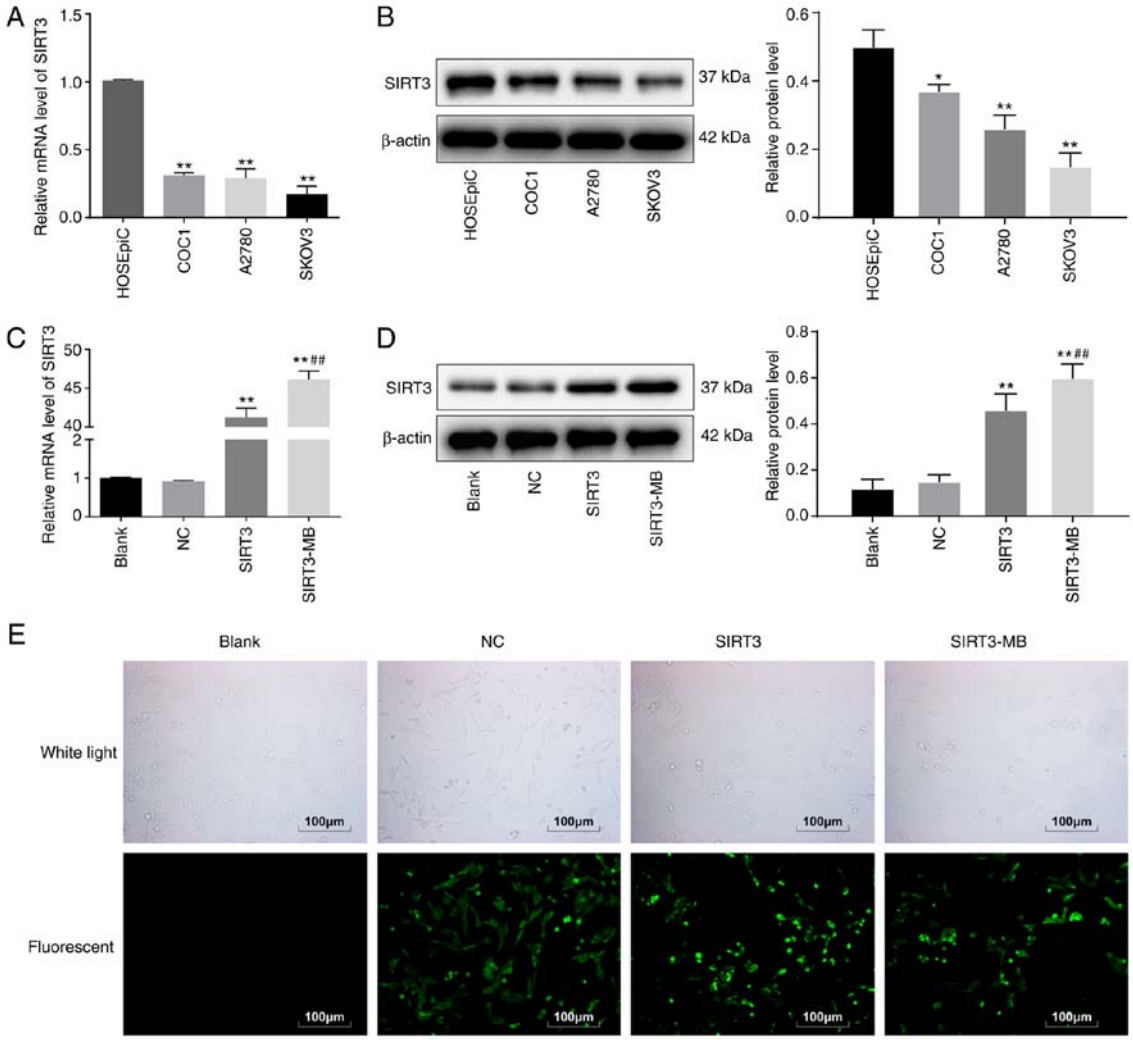


Figure 1. Relative expression levels of SIRT3 and the validation of the effectiveness of vector transfection. (A) The relative mRNA expression levels of SIRT3 in the HOC cell lines COC1, A2780 and SKOV3, and in the ovarian epithelial cell line HOSEpiC were measured via RT-qPCR. (B) Relative protein expression levels of SIRT3 in the HOC and the HOSEpiC cell lines were determined by western blotting. (C) Relative SIRT3 mRNA expression was detected by RT-qPCR after SIRT3 transfection or SIRT3-MB transfection with ultrasound treatment. (D) Relative SIRT3 protein expression was detected by western blot analysis after SIRT3 transfection or SIRT3-MB transfection with ultrasound treatment. (E) GFP fluorescence for the detection of recombinant SIRT3 vector transfection. The data are expressed as the mean ± standard deviation and were compared using one-way ANOVA and Tukey's multiple comparisons test. $^{*}$P<0.05 and $^{**}$P<0.01 vs. HOSEpic or Blank; $^{\#\#}$P<0.01 vs. SIRT3. GFP, green fluorescent protein; HOC, human ovarian cancer; MB, microbubble; NC, negative control; RT-qPCR, reverse transcription-quantitative PCR; SIRT3, Sirtuin 3.

*Statistical analysis*. The Statistical Package for the Social Sciences version 21.0 (IBM Corp.) was used for data analysis. The normality test was conducted using the Kolmogorov-Smirnov method. Measurement data were in normal distribution and are expressed as mean ± standard deviation. Differences among multiple groups were compared using one-way followed by Tukey's post hoc test for pairwise comparisons. The P-value was obtained from a two-tailed test and P<0.05 was considered to indicate a statistically significant difference.

## Results

*SIRT3 is expressed at low levels in HOC cells*. The expression of SIRT3 mRNA in the HOC cell lines COC1, A2780 and SKOV3 and human ovarian epithelial cells HOSEpiC was detected by RT-qPCR, the results of which indicated that the *SIRT3* mRNA levels in HOC cells were significantly lower compared with that in HOSEpiC (P<0.01; Fig. 1A). SIRT3 protein expression in cells exhibited a similar trend according to western blot analysis (P<0.05; Fig. 1B). Among the cell lines, SKOV3 cells had the lowest SIRT3 expression and were selected for the subsequent experiments.

After transfecting the pLVX-SIRT3-IRES-ZsGreen1 vector into SKOV3 cells for 48 h, the mRNA expression of *SIRT3* was significantly increased compared with Blank (P<0.01; Fig. 1C). Moreover, western blot analysis demonstrated that SIRT3 protein expression was also increased (P<0.01; Fig. 1D). Under a fluorescence microscope, the cells presented with green fluorescence (Fig. 1E), and the transfection efficiency exceeded 80%, indicating that a SKOV3 cell line overexpressing SIRT3 was successfully constructed. When SKOV3 cells were treated with SIRT3-MB, SIRT3 mRNA (P<0.01; Fig. 1C) and protein (P<0.05; Fig. 1D) expression levels were further increased compare with the SIRT3 group; the cells also exhibited green fluorescence (Fig. 1E). It was suggested that ultrasound microbubbles could further promote the transfection efficiency of SIRT3 plasmid.

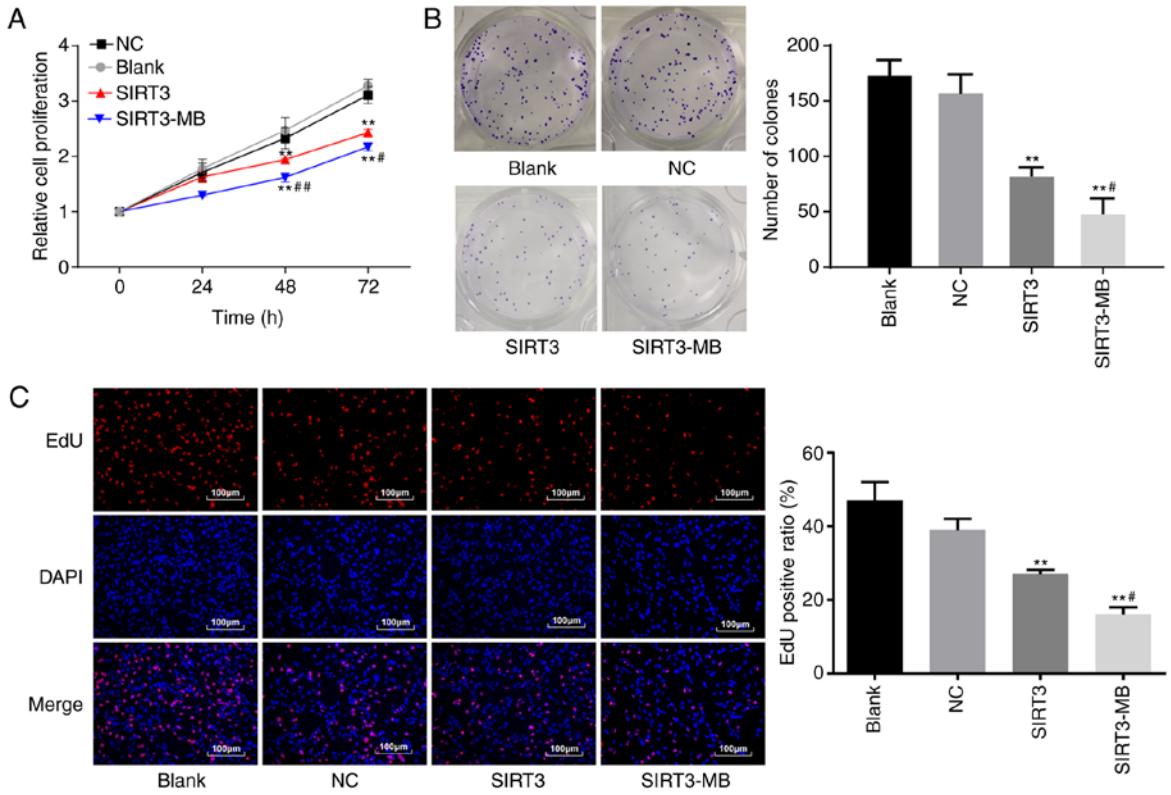


Figure 2. Ultrasound-targeted microbubble destruction-mediated *SIRT3* inhibits SKOV3 cell proliferation. (A) SKOV3 proliferation was detected using an MTT assay. (B) SKOV3 proliferation was also detected by a colony formation assay. (C) SKOV3 DNA replication was detected using an EdU assay. The data are expressed as the mean ± standard deviation and were compared using one-way ANOVA, followed by Tukey's multiple comparisons test. $^{**}$P<0.01 vs. Blank; $^{\#}$P<0.05 and $^{\#\#}$P<0.01 vs. SIRT3. EdU, 5-ethynyl-2'-deoxyuridine labeling assay; MB, microbubble; NC, negative control; SIRT3, Sirtuin 3.

*UTMD-mediated overexpression of SIRT3 inhibits the proliferation of SKOV3 cells in vitro*. Cell proliferation was measured by an MTT assay. No significant difference was observed between the NC group and the blank group (P>0.05), whereas cell proliferation rates at 48 (P<0.01) and 72 h (P<0.01) were significantly lower in the SIRT3 group compared with the blank and NC groups (Fig. 2A). Cells in the SIRT3-MB group after UTMD treatment showed further reduced cell proliferation rates compared with the SIRT3 group at 48 and 72 h (P<0.01 and P<0.05, respectively).

The colony formation ability of SKOV3 cells was measured (Fig. 2B). No significant difference was observed in the number of clones between the blank group and the NC group (P>0.05); however, compared with the blank group, the number of clones was significantly reduced in the SIRT3 group (P<0.01). After UTMD treatment, cells in the SIRT3-MB group showed more significantly decreased cell clones compared with the SIRT3 group (P<0.05; Fig. 2B). The results above indicated that overexpression of SIRT3 could inhibit the proliferation of SKOV3 cells *in vitro*.

The EdU assay was used to measure the DNA replication activity, the results of which demonstrated that the DNA replication activity of cells in the blank and NC groups were not significantly different in the rate of EdU-positive cells (Fig. 2C). The DNA replication activity in the cells overexpressing *SIRT3* was significantly decreased compared with the blank group (P<0.01). After UTMD treatment, cells in the SIRT3-MB group showed a further decrease in the number of EdU-positive cells compared with the SIRT3 group (P<0.05; Fig. 2C).

*UTMD-mediated overexpression of SIRT3 inhibits the epithelial-mesenchymal transition (EMT) of SKOV3 cells*. EMT is a phenotypic change closely related to tumor metastasis. EMT is usually marked by decreased expression of E-cadherin and increased expression of N-cadherin and Vimentin (25). The results of RT-qPCR revealed that the mRNA expression levels of *E-cadherin* in the SIRT3 group were significantly increased compared with those in the blank and NC groups (P<0.01), whereas the mRNA expression levels of *N-cadherin* and *Vimentin* were significantly decreased (P<0.01) (Fig. 3A). Moreover, after UTMD treatment, cells in the SIRT3-MB group demonstrated further elevated *E-cadherin* mRNA expression (P<0.01), as well as further decreased *N-cadherin* (P<0.01) and *Vimentin* (P<0.05) mRNA expression compared with the SIRT3 group (Fig. 3A). Similar trends in protein expression levels were observed by western blot analysis (Fig. 3B). These results suggested that overexpression of SIRT3 may inhibit EMT of SKOV3 cells.

*UTMD-mediated overexpression of SIRT3 suppresses the migration and invasion of SKOV3 cells*. Malignant tumors are characterized by the ability to invade and migrate (26). Therefore, the invasive and migratory abilities of SKOV3 cells were determined by *in vitro* Matrigel and wound healing experiments, respectively. The results demonstrated that cell invasion (P<0.01) and migration (P<0.01) were significantly decreased in the SIRT3 group compared with the blank and NC groups (Fig. 4A and B). After UTMD treatment, SKOV3 cells in the SIRT3-MB group demonstrated further decreases

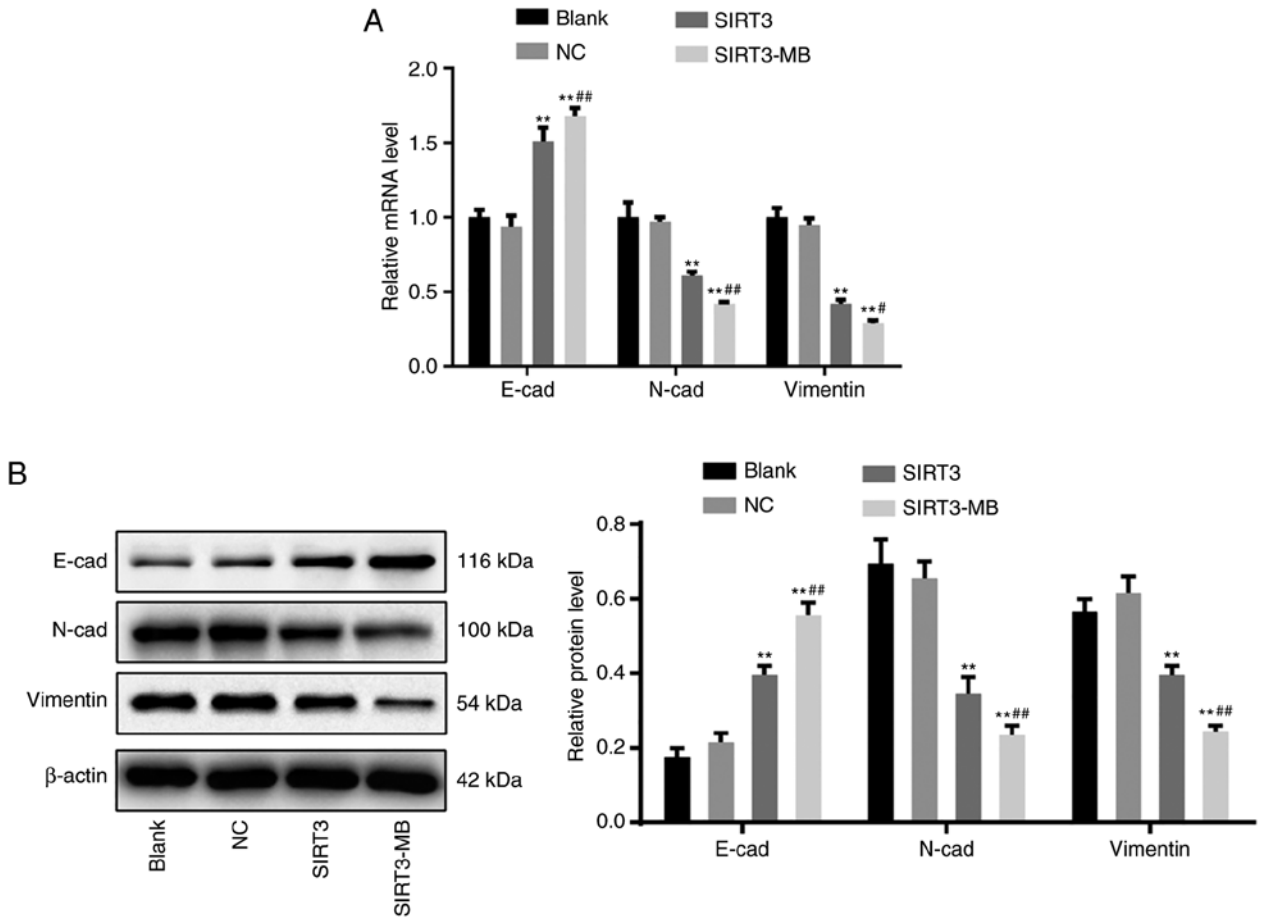


Figure 3. Ultrasound-targeted microbubble destruction-mediated *SIRT3* overexpression inhibits epithelial-mesenchymal transition. (A) mRNA and (B) protein expression levels of E-cadherin, N-cadherin and Vimentin were measured by reverse transcription-quantitative PCR and western blot analysis, respectively. The data are expressed as the mean ± standard deviation and were compared using one-way ANOVA and Tukey's multiple comparisons test. $^{**}$P<0.01 vs. Blank; $^{\#}$P<0.05 and $^{\#\#}$P<0.01 vs. SIRT3 group. MB, microbubble; NC, negative control; SIRT3, Sirtuin 3.

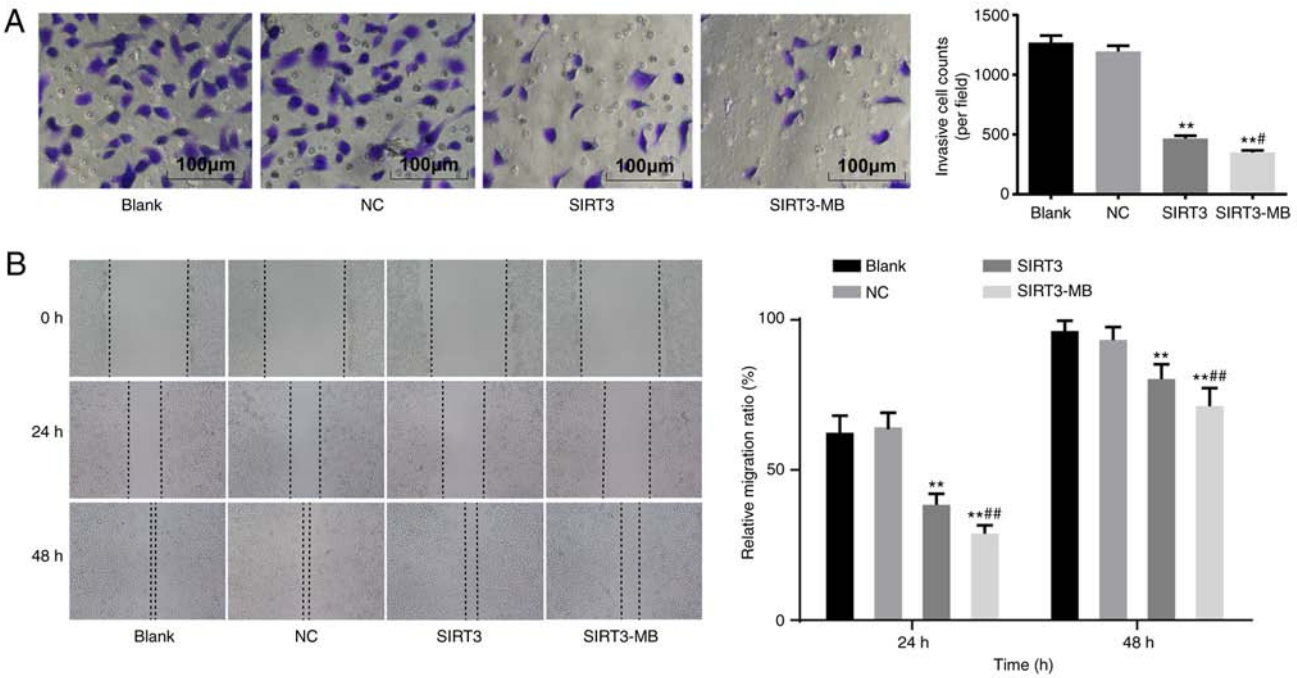


Figure 4. Ultrasound-targeted microbubble destruction-mediated *SIRT3* overexpression suppresses SKOV3 cell invasion and migration. (A) Cell invasion was detected by *in vitro* Matrigel invasion experiments. (B) Cell migratory ability was detected using *in vitro* wound healing experiments. The data are expressed as the mean ± standard deviation and were compared using one-way ANOVA, followed by Tukey's multiple comparisons test. $^{**}$P<0.01 vs. Blank; $^{\#}$P<0.05, $^{\#\#}$P<0.01 vs. SIRT3. MB, microbubble; NC, negative control; SIRT3, Sirtuin 3.

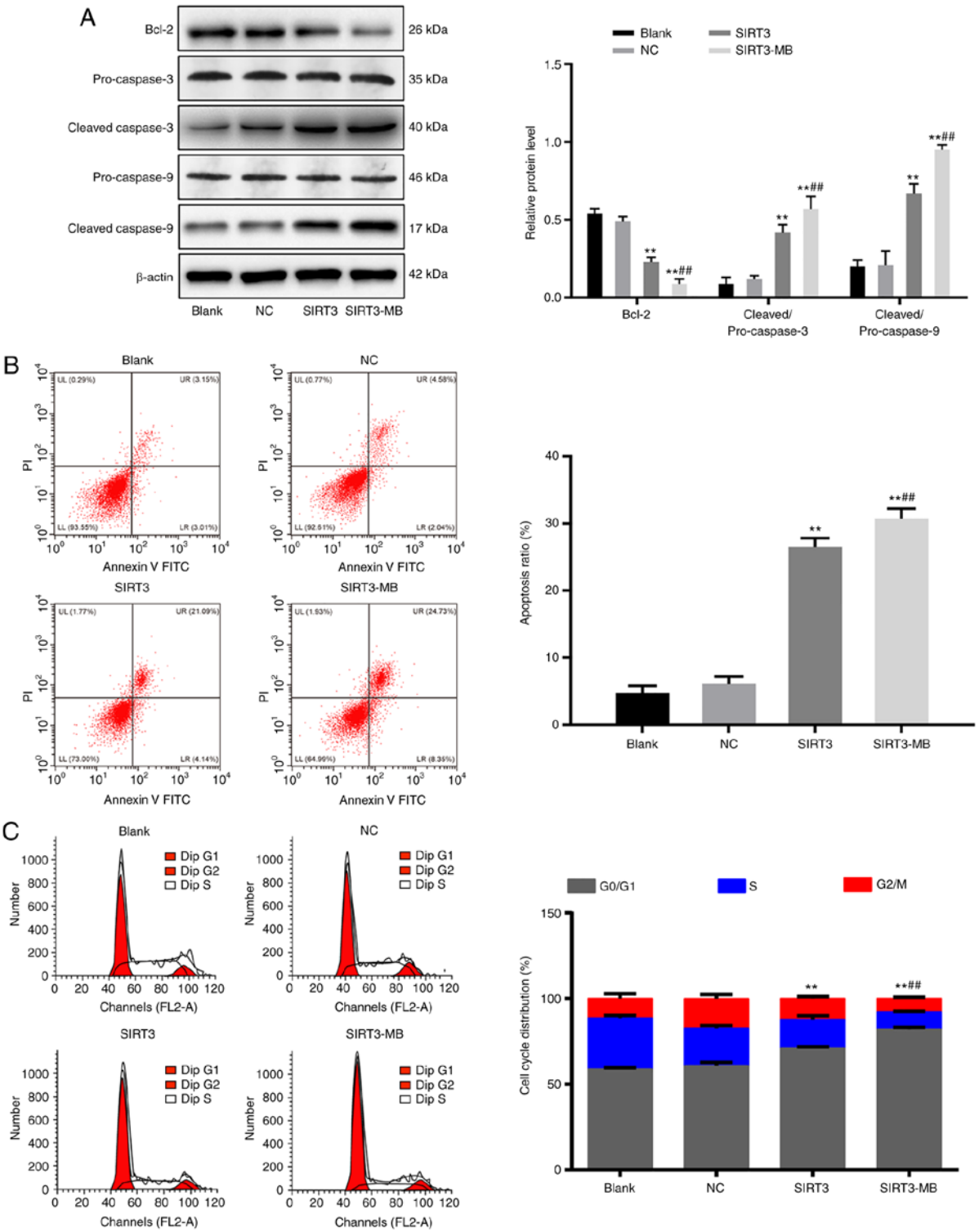


Figure 5. UTMD-mediated *SIRT3* induces apoptosis and cell cycle arrest. (A) Protein expression levels of the apoptosis-related proteins cleaved caspase-3, pro-caspase-3, cleaved caspase-9, pro-caspase-9 and Bcl-2 were detected by western blot analysis. (B) Apoptosis of SKOV3 cells was detected by flow cytometry. (C) Following SIRT3transfection and UTMD treatment, the cell cycle of SKOV3 cells measured by flow cytometry. The data are expressed as the mean ± standard deviation and were compared using one-way ANOVA, followed by Tukey's multiple comparisons test. $^{**}$P<0.01 vs. Blank; $^{\#\#}$P<0.01 vs. SIRT3. MB, microbubble; NC, negative control; SIRT3, Sirtuin 3; UTMD, ultrasound-targeted microbubble destruction.

in invasion (P<0.05) and migration (P<0.01) compared with those in the SIRT3 group (Fig. 4A and B).

*UTMD-mediated overexpression of SIRT3 promotes apoptosis and cell cycle arrest in SKOV3 cells*. The protein expression levels of cell apoptosis-related proteins, including cleaved caspase-3, pro-caspase-3, Bcl-2, cleaved caspase-9 and pro-caspase-9 were measured by western blot analysis. No significant difference was observed in the protein expression levels of the above factors between the blank and NC groups (Fig. 5A). Compared with those in the blank group, the protein ratio levels of cleaved/pro-caspase-3

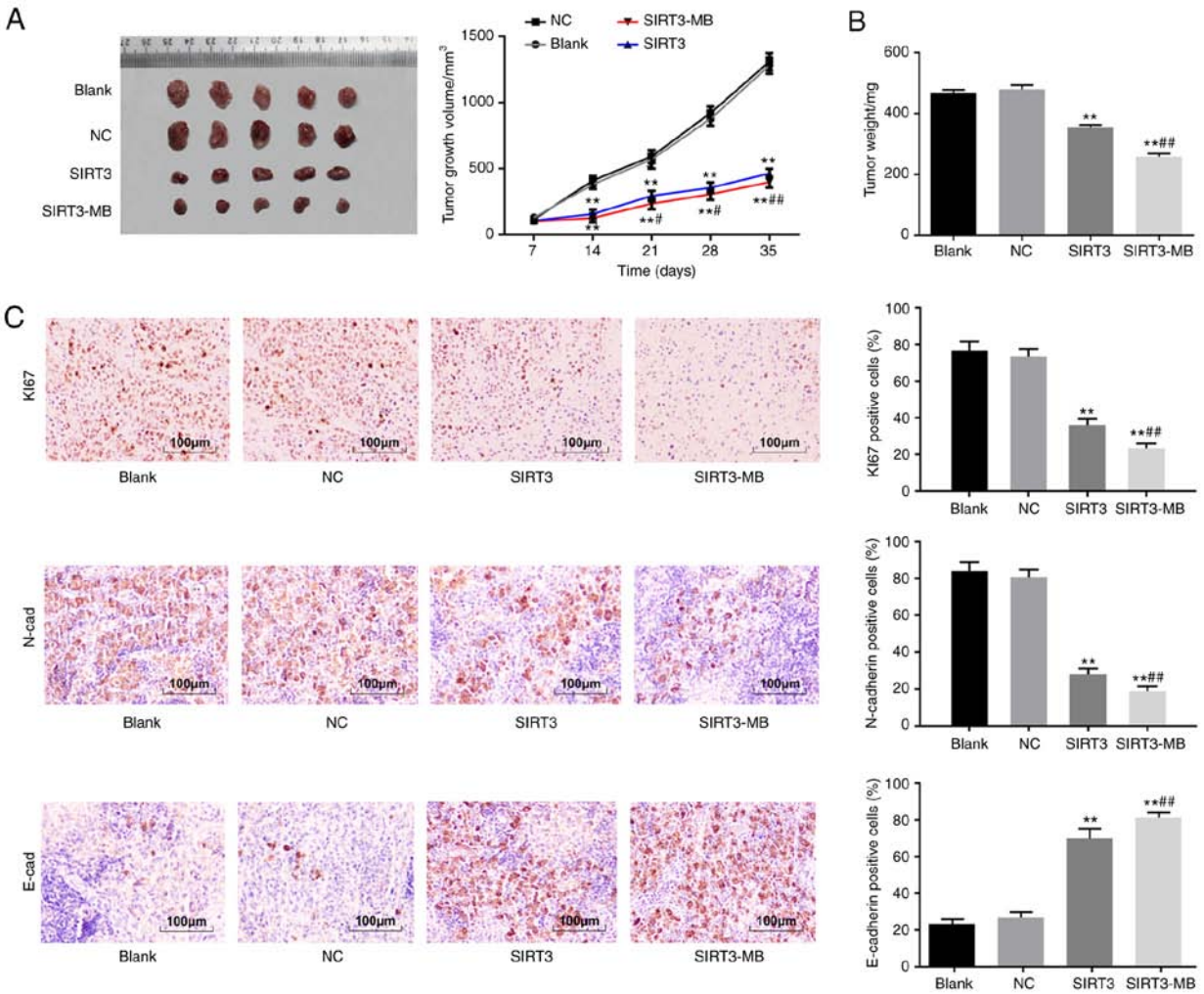


Figure 6. Ultrasound-targeted microbubble destruction-mediated *SIRT3* inhibits the growth of SKOV3 xenograft tumors. (A) Volume and (B) weight of SKOV3 xenografted tumors *in vivo*. (C) Immunohistochemical analysis forKi67, E-cadherin and N-cadherin performed on SKOV3 xenograft tumors. Brown color indicates positive expression; the blue color indicated stained nuclei. The data are expressed as the mean ± standard deviation and were compared using one-way ANOVA, followed by Tukey's multiple comparisons test. $^{**}$P<0.01 vs. Blank; $^{\#}$P<0.05 and $^{\#\#}$P<0.01 vs. SIRT3. MB, microbubble; NC, negative control; SIRT3, Sirtuin 3.

and cleaved/pro-caspase-9 were significantly increased in the SIRT3 group (P<0.01), whereas the level of Bcl-2 was decreased (P<0.01). After UTMD treatment, the protein ratio levels of cleaved/pro-caspase-3 and cleaved/pro-caspase-9 were further increased, whereas the Bcl-2 protein level was further decreased in the SIRT3-MB group, compared with the SIRT3 group (all P<0.01; Fig. 5A).

Flow cytometry was performed to detect cell apoptosis (early + late) and cell cycle progression, and the results showed that, compared with blank and NC groups, the number of early apoptotic cells was increased (P<0.01; Fig. 5B), G2/M cells were decreased (P<0.01), and G0/G1 cells were increased significantly in SIRT3 group (P<0.01) (Fig. 5C). Compared with that in the SIRT3 group, cell apoptosis was significantly increased in the SIRT3-MB group (P<0.01). Fewer cells were detected in the G2/M phase (P<0.01), whereas significantly more cells were found in G0/G1 phase (P<0.01).

*UTMD-mediated overexpression of SIRT3 inhibits tumorigenesis of SKOV3 cells in vivo*. A nude mouse model with SKOV3 xenograft tumors was established, and the effect of SIRT3 on the *in vivo* growth of these cells was evaluated by measuring tumor volume and weight. The results revealed that the volume of xenograft tumors (after day 14) in the SIRT3 and SIRT3-MB groups was significantly smaller compared with those in mice in the blank and NC groups; xenograft tumor growth inhibition was more pronounced in the SIRT3-MB group (all P<0.05; Fig. 6A). On day 35, the largest tumor volume of nude mice was 1,430 $mm^3$. Tumor weight was inhibited in the SIRT3 group compared with the blank and NC groups (P<0.01), and further inhibited in the SIRT3-MB group compared with SIRT3 group (P<0.01) (Fig. 6B).

Ki67 is an antigen associated with cell proliferation. The results of the immunohistochemistry demonstrated that, compared with those in the blank and NC groups, the number of Ki67- and N-cadherin-expressing cells were significantly decreased in the SIRT3 group, whereas the number of E-cadherin-positive cells was increased (P<0.01; Fig. 6C). In the SIRT3-MB group, the number of Ki67- and N-cadherin-positive cells in tumor tissues were further decreased, and the positive-expression rate of E-cadherin was further increased compared with that in the SIRT3 group (all P<0.01; Fig. 6C). These results indicated that UTMD-mediated overexpression of SIRT3 may inhibit tumorigenesis of SKOV3 cells *in vivo*.

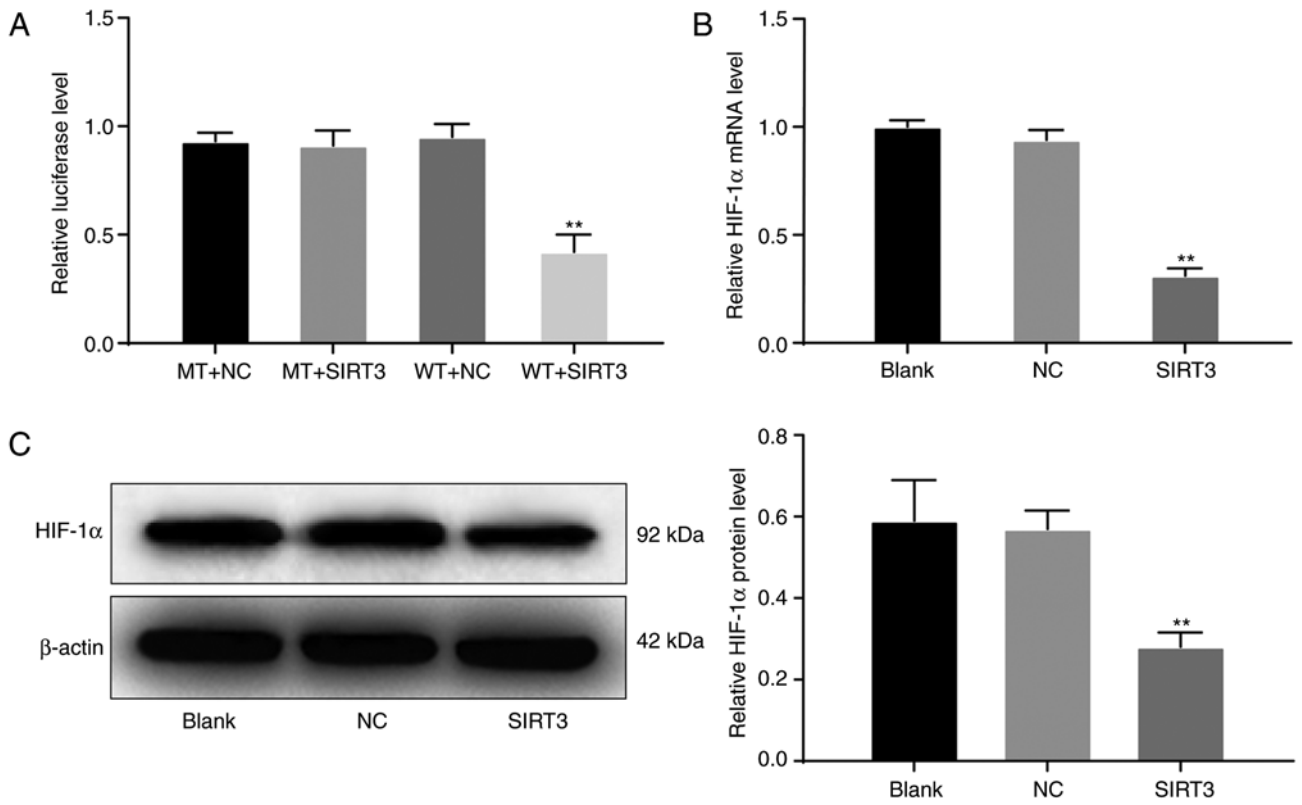


Figure 7. *SIRT3* regulates HIF-1α expression. (A) Luciferase activity in each group was detected by the dual luciferase reporter assay. (B) mRNA and (C) protein expression levels of HIF-1α in SKOV3 cells were detected by reverse transcription-quantitative PCR and western blot analysis, respectively. The data are expressed as the mean ± standard deviation and were compared using one-way ANOVA, followed by Tukey's multiple comparisons test. **P<0.01 vs. WT + NC or Blank. HIF-1α, hypoxia inducible factor-1α; MT, mutant-type; NC, negative control; SIRT3, Sirtuin 3; WT, wild-type.

*SIRT3 may inhibit the growth of HOC SKOV3 cells by regulating HIF-1α*. HIF-1α is a cytokine produced in response to tumor hypoxia. Under hypoxic conditions, the HIF-1α signaling pathway is activated, inducing a range of cellular activities, such as metabolism, inflammatory response, angiogenesis, and tumor formation. The HIF-1α signaling pathway was found in many tumors, including HOC (27). Therefore, combining these observations with those aforementioned, we hypothesized that SIRT3 may inhibit the growth of HOC cells by regulating the HIF-1α signaling pathway. The dual luciferase assay results demonstrated that there was no significant difference in luciferase activity among the MT + SIRT3, MT + NC and WT + NC groups, whereas the luciferase activity in the WT + SIRT3 group was significantly decreased (P<0.01; Fig. 7A). The results of RT-qPCR revealed that the mRNA expression levels of HIF-1α in the SIRT3 group was significantly decreased compared with that in the blank and NC groups (P<0.01; Fig. 7B). Similarly, western blot analysis results revealed that, compared with the expression in the blank and NC groups, the protein expression levels of HIF-1α in the SIRT3 group was significantly decreased (P<0.01; Fig. 7C). These results suggested that *SIRT3* may inhibit the growth of HOC cells by regulating the HIF-1α signaling pathway.

## Discussion

HOC remains one of the leading causes of cancer-related mortalities among patients with gynecologic malignancies (28). SIRT3 has roused wide interest in cancer treatment as it could serve as either a tumor suppressor or promoter in different cases (8). UTMD has been suggested as a promising non-invasive tool for site-specific gene delivery allowing direct transfection into cells (29,30). In the present study, the role of SIRT3 in the malignant behaviors of HOC cells was investigated, and it was found that UTMD-mediated overexpression of *SIRT3* could reduce the malignant behaviors of SKOV3 cells, possibly by downregulating HIF-1α.

In the present study, low expression of *SIRT3* was demonstrated in SKOV3 cells. Following UTMD treatment, *SIRT3* expression was significantly elevated and led to reduced cell proliferation, migration and invasion, as well as decreased Ki67, Vimentin and N-cadherin expression and increased E-cadherin expression, in addition to increased expression of caspase-3 and caspase-9. However, decreased expression of Bcl-2 was demonstrated. Ki67 is an important proliferation marker and is activated during all phases in the cell cycle (31). E-cadherin is a cell junction protein that is downregulated or silenced, whereas Vimentin expression is usually increased during EMT progression (32). Bcl-2 is an anti-apoptotic protein whose high expression has been suggested to be frequently presented in human cancers and closely associated with resistance to chemotherapies and cancer development (33); caspase-3 and caspase-9 are well-known apoptosis inducers (34). Moreover, the present study revealed that UTMD further prompted the inhibitory effect of SIRT3 on SKOV3 cells and further suppressed tumor growth *in vivo*. UTMD has emerged rapidly in recent years as a novel technique for gene therapy that shows potential

for wide use in gene therapy and cell biology. For instance, UTMD combined with liposomes has been suggested to promote short hairpin (sh)RNA transfection efficiency into cells to inhibit metadherin expression, thus leading to the downregulation of proliferation and metastatic processes in MCF-7 breast cancer cells (35). Similarly, UTMD-mediated HIF-1 shRNA transfection has served an enhancing role in tumor growth inhibition (36). The results of the present study demonstrated that UTMD upregulated *SIRT3* expression and further suppressed the malignant behaviors of SKOV3 cells. *SIRT3* has been demonstrated to serve as either a tumor suppressor or tumor promoter in different malignancies (37). For example, SIRT3 was found to be expressed at low levels in human gastric cancer and to inhibit cell proliferation (38). In addition, SIRT3 has been reported to inhibit the development of prostate cancer (13). Conversely, its tumor promoting role has also been revealed in several malignancies, including cervical cancer (39) and breast cancer cells (40). In the present study, *SIRT3* inhibited SKOV3 HOC cell proliferation, invasion, migration, EMT and resistance to apoptosis, with an inhibitory effect found on tumor growth in nude mice. *SIRT3* was previously reported to be downregulated in HOC cell lines and inhibited in cell metastasis and invasion (41). Similarly, downregulation of *SIRT3* has been found to promote OC metastasis (42). Based on these data, *SIRT3* may serve as a potential therapeutic option for HOC control and treatment.

These findings prompted the authors of the present study to further identify the potential molecular mechanism involved in HOC progression. Importantly, the dual luciferase reporter gene assay results suggested that *SIRT3* could directly bind to HIF-1α. Similarly, RT-qPCR and western blot analysis revealed that *SIRT3* overexpression led to decreased HIF-1α mRNA and protein expression in SKOV3 cells. HIF-1α can initiate angiogenesis, and upregulation of the HIF-1α pathway has been found in various cancers caused by different environmental factors (43). HIF-1α is closely associated with the malignancy of ovarian tumors, and the downregulation of HIF-1α expression could result in a decreased proliferation of ovarian cells (44). Overexpressed *SIRT3* has been demonstrated to reduce HIF-1α protein stabilization in hypoxia and reverse the increases in the transcriptional activity of HIF-1α to inhibit colon cancer tumorigenesis (45). Hence, it could be inferred that *SIRT3* might inhibit the progression of HOC through the downregulation of HIF-1α.

In summary, the present study demonstrated that *SIRT3* was expressed at low levels in HOC cells. Upregulation of *SIRT3* inhibited HOC cell proliferation, invasion, EMT and *in vivo* tumor growth, and promoted cell apoptosis and cell cycle arrest. UTMD further strengthened the inhibitory effect of *SIRT3* overexpression on HOC growth *in vivo* and *in vitro*. Downregulation of HIF-1α might be involved in the above events, as it was demonstrated that *SIRT3* led to decreased HIF-1α expression in SKOV3 cells. Future studies will explore more detailed links between *SIRT3* and HIF-1α expression and will determine additional molecular mechanisms involved in the effect of *SIRT3* on HIF-1α. These findings may provide novel insights into HOC control and treatment, and additional studies in this field are required to develop additional therapeutic options for HOC and other severe diseases.

**Acknowledgements**

Not applicable.

**Funding**

Not applicable.

**Availability of data and materials**

All data generated and analyzed during this study are included in this published article.

**Authors' contributions**

LC and DZ designed the study. LC carried out the analytical assays. WY performed the statistical analyses. LC drafted the manuscript. All authors read and approved the final manuscript.

**Ethics approval and consent to participate**

The present study was performed with the approval of the Ethics Committee of The Affiliated Hospital of Changchun University of Traditional Chinese Medicine (Jilin, China).

**Patient consent for publication**

Not applicable.

**Competing interests**

The authors declare that they have no competing interests.

**References**

1. Hua F, Li CH, Chen XG and Liu XP: Daidzein exerts anticancer activity towards SKOV3 human ovarian cancer cells by inducing apoptosis and cell cycle arrest and inhibiting the Raf/MEK/ERK cascade. Int J Mol Med 41: 3485-3492, 2018.
2. Bareiss PM, Paczulla A, Wang H, Schairer R, Wiehr S, Kohlhofer U, Rothfuss OC, Fischer A, Perner S, Staebler A, *et al*: SOX2 expression associates with stem cell state in human ovarian carcinoma. Cancer Res 73: 5544-5555, 2013.
3. Wolterink S, Moldenhauer G, Fogel M, Kiefel H, Pfeifer M, Lüttgau S, Gouveia R, Costa J, Endell J, Moebius U and Altevogt P: Therapeutic antibodies to human L1CAM: Functional characterization and application in a mouse model for ovarian carcinoma. Cancer Res 70: 2504-2515, 2010.
4. Zhang S, Xie B, Wang L, Yang H, Zhang H, Chen Y, Wang F, Liu C and He H: Macrophage-mediated vascular permeability via VLA4/VCAM1 pathway dictates ascites development in ovarian cancer. J Clin Invest 131: e140315, 2021.
5. Campbell S and Gentry-Maharaj A: The role of transvaginal ultrasound in screening for ovarian cancer. Climacteric 21: 221-226, 2018.
6. Varughese J, Cocco E, Bellone S, Bellone M, Todeschini P, Carrara L, Schwartz PE, Rutherford TJ, Pecorelli S and Santin AD: High-grade, chemotherapy-resistant primary ovarian carcinoma cell lines overexpress human trophoblast cell-surface marker (Trop-2) and are highly sensitive to immunotherapy with hRS7, a humanized monoclonal anti-Trop-2 antibody. Gynecol Oncol 122: 171-177, 2011.
7. Alhazzazi TY, Kamarajan P, Joo N, Huang JY, Verdin E, D'Silva NJ and Kapila YL: Sirtuin-3 (SIRT3), a novel potential therapeutic target for oral cancer. Cancer 117: 1670-1678, 2011.

8. Taylor DM, Maxwell MM, Luthi-Carter R and Kazantsev AG: Biological and potential therapeutic roles of sirtuin deacetylases. Cell Mol Life Sci 65: 4000-4018, 2008.
9. Alhazzazi TY, Kamarajan P, Verdin E and Kapila YL: SIRT3 and cancer: Tumor promoter or suppressor? Biochim Biophys Acta 1816: 80-88, 2011.
10. Desouki MM, Doubinskaia I, Gius D and Abdulkadir SA: Decreased mitochondrial SIRT3 expression is a potential molecular biomarker associated with poor outcome in breast cancer. Hum Pathol 45: 1071-1077, 2014.
11. Kim HS, Patel K, Muldoon-Jacobs K, Bisht KS, Aykin-Burns N, Pennington JD, van der Meer R, Nguyen P, Savage J, Owens KM, *et al*: SIRT3 is a mitochondria-localized tumor suppressor required for maintenance of mitochondrial integrity and metabolism during stress. Cancer Cell 17: 41-52, 2010.
12. Yang B, Fu X, Shao L, Ding Y and Zeng D: Aberrant expression of SIRT3 is conversely correlated with the progression and prognosis of human gastric cancer. Biochem Biophys Res Commun 443: 156-160, 2014.
13. Quan Y, Wang N, Chen Q, Xu J, Cheng W, Di M, Xia W and Gao WQ: SIRT3 inhibits prostate cancer by destabilizing oncoprotein c-MYC through regulation of the PI3K/Akt pathway. Oncotarget 6: 26494-26507, 2015.
14. Carson AR, McTiernan CF, Lavery L, Hodnick A, Grata M, Leng X, Wang J, Chen X, Modzelewski RA and Villanueva FS: Gene therapy of carcinoma using ultrasound-targeted microbubble destruction. Ultrasound Med Biol 37: 393-402, 2011.
15. Chen S and Grayburn PA: Ultrasound-targeted microbubble destruction for cardiac gene delivery. Methods Mol Biol 1521: 205-218, 2017.
16. Villanueva FS: Ultrasound mediated destruction of DNA-loaded microbubbles for enhancement of cell-based therapies: New promise amidst a confluence of uncertainties? JACC Cardiovasc Imaging 2: 880-882, 2009.
17. Gao F, Wu J, Niu S, Sun T, Li F, Bai Y, Jin L, Lin L, Shi Q, Zhu LM and Du L: Biodegradable, pH-sensitive hollow mesoporous organosilica nanoparticle (HMON) with controlled release of pirfenidone and ultrasound-target-microbubble-destruction (UTMD) for pancreatic cancer treatment. Theranostics 9: 6002-6018, 2019.
18. Jing H, Cheng W, Li S, Wu B, Leng X, Xu S and Tian J: Novel cell-penetrating peptide-loaded nanobubbles synergized with ultrasound irradiation enhance EGFR siRNA delivery for triple negative breast cancer therapy. Colloids Surf B Biointerfaces 146: 387-395, 2016.
19. Zhong S, Shu S, Wang Z, Luo J, Zhong W, Ran H, Zheng Y, Yin Y and Ling Z: Enhanced homing of mesenchymal stem cells to the ischemic myocardium by ultrasound-targeted microbubble destruction. Ultrasonics 52: 281-286, 2012.
20. Livak KJ and Schmittgen TD: Analysis of relative gene expression data using real-time quantitative PCR and the 2(-Delta Delta C(T)) method. Methods 25: 402-408, 2001.
21. Naito S, von Eschenbach AC, Giavazzi R and Fidler IJ: Growth and metastasis of tumor cells isolated from a human renal cell carcinoma implanted into different organs of nude mice. Cancer Res 46: 4109-4115, 1986.
22. Zatroch KK, Knight CG, Reimer JN and Pang DS: Refinement of intraperitoneal injection of sodium pentobarbital for euthanasia in laboratory rats (Rattus norvegicus). BMC Vet Res 13: 60, 2017.
23. Kopaladze RA: Methods for the euthanasia of experimental animals-the ethics, esthetics and personnel safety. Usp Fiziol Nauk 31: 79-90, 2000 (In Russian).
24. Yao W, Ji S, Qin Y, Yang J, Xu J, Zhang B, Xu W, Liu J, Shi S, Liu L, *et al*: Profilin-1 suppresses tumorigenicity in pancreatic cancer through regulation of the SIRT3-HIF1α axis. Mol Cancer 13: 187, 2014.
25. Paolillo M and Schinelli S: Extracellular matrix alterations in metastatic processes. Int J Mol Sci 20: 4947, 2019.
26. Brown GT and Murray GI: Current mechanistic insights into the roles of matrix metalloproteinases in tumour invasion and metastasis. J Pathol 237: 273-281, 2015.
27. Hu Y, Liu J and Huang H: Recent agents targeting HIF-1α for cancer therapy. J Cell Biochem 114: 498-509, 2013.
28. Hamanishi J, Mandai M, Ikeda T, Minami M, Kawaguchi A, Murayama T, Kanai M, Mori Y, Matsumoto S, Chikuma S, *et al*: Safety and antitumor activity of anti-PD-1 antibody, nivolumab, in patients with platinum-resistant ovarian cancer. J Clin Oncol 33: 4015-4022, 2015.
29. Chen ZY, Liang K, Sheng XJ, Si-Tu B, Sun XF, Liu JQ, Qiu RX, Zhang H, Li YW, Zhou XX and Yu JX: Optimization and apoptosis induction by RNAi with UTMD technology *in vitro*. Oncol Lett 3: 1030-1036, 2012.
30. Su J, Wang J, Luo J and Li H: Ultrasound-mediated destruction of vascular endothelial growth factor (VEGF) targeted and paclitaxel loaded microbubbles for inhibition of human breast cancer cell MCF-7 proliferation. Mol Cell Probes 46: 101415, 2019.
31. Stromar IK and Jakic-Razumovic J: The value of immunohistochemical determination of topoisomerase IIα and Ki67 as markers of cell proliferation and malignant transformation in colonic mucosa. Appl Immunohistochem Mol Morphol 22: 524-529, 2014.
32. Zhao J, Dong D, Sun L, Zhang G and Sun L: Prognostic significance of the epithelial-to-mesenchymal transition markers e-cadherin, vimentin and twist in bladder cancer. Int Braz J Urol 40: 179-189, 2014.
33. Xiang XY, Kang JS, Yang XC, Su J, Wu Y, Yan XY, Xue YN, Xu Y, Liu YH, Yu CY, *et al*: SIRT3 participates in glucose metabolism interruption and apoptosis induced by BH3 mimetic S1 in ovarian cancer cells. Int J Oncol 49: 773-784, 2016.
34. Liu J, Yao Y, Ding H and Chen R: Oxymatrine triggers apoptosis by regulating Bcl-2 family proteins and activating caspase-3/caspase-9 pathway in human leukemia HL-60 cells. Tumour Biol 35: 5409-5415, 2014.
35. Xu J, Wang Y, Li Z, Wang Q, Zhou X and Wu W: Ultrasound-targeted microbubble destruction (UTMD) combined with liposome increases the effectiveness of suppressing proliferation, migration, invasion, and epithelial-mesenchymal transition (EMT) via targeting metadherin (MTDH) by ShRNA. Med Sci Monit 25: 2640-2648, 2019.
36. Liao Y, Luo H, He Z, Kuang Y, Chen P, Zhang X, Chen J, Wen Q, Xie Y and Ding S: A combination of UTMD-mediated HIF-1 α shRNA transfection and TAE in the treatment of hepatic cancer. Biomed Res Int 2019: 1937460, 2019.
37. Chen Y, Fu LL, Wen X, Wang XY, Liu J, Cheng Y and Huang J: Sirtuin-3 (SIRT3), a therapeutic target with oncogenic and tumor-suppressive function in cancer. Cell Death Dis 5: e1047, 2014.
38. Wang L, Wang WY and Cao LP: SIRT3 inhibits cell proliferation in human gastric cancer through down-regulation of notch-1. Int J Clin Exp Med 8: 5263-5271, 2015.
39. Xu LX, Hao LJ, Ma JQ, Liu JK and Hasim A: SIRT3 promotes the invasion and metastasis of cervical cancer cells by regulating fatty acid synthase. Mol Cell Biochem 464: 11-20, 2019.
40. Zhang L, Ren X, Cheng Y, Huber-Keener K, Liu X, Zhang Y, Yuan YS, Yang JW, Liu CG and Yang JM: Identification of sirtuin 3, a mitochondrial protein deacetylase, as a new contributor to tamoxifen resistance in breast cancer cells. Biochem Pharmacol 86: 726-733, 2013.
41. Dong XC, Jing LM, Wang WX and Gao YX: Down-regulation of SIRT3 promotes ovarian carcinoma metastasis. Biochem Biophys Res Commun 475: 245-250, 2016.
42. Wu Y, Gao WN, Xue YN, Zhang LC, Zhang JJ, Lu SY, Yan XY, Yu HM, Su J and Sun LK: SIRT3 aggravates metformin-induced energy stress and apoptosis in ovarian cancer cells. Exp Cell Res 367: 137-149, 2018.
43. Boreddy SR, Sahu RP and Srivastava SK: Benzyl isothiocyanate suppresses pancreatic tumor angiogenesis and invasion by inhibiting HIF-α/VEGF/Rho-GTPases: Pivotal role of STAT-3. PLoS One 6: e25799, 2011.
44. Fujita M, Yasuda M, Kitatani K, Miyazawa M, Hirabayashi K, Takekoshi S, Iida T, Hirasawa T, Murakami M, Mikami M, *et al*: An up-to-date anti-cancer treatment strategy focusing on HIF-1alpha suppression: Its application for refractory ovarian cancer. Acta Histochem Cytochem 40: 139-142, 2007.
45. Bell EL, Emerling BM, Ricoult SJ and Guarente L: SirT3 suppresses hypoxia inducible factor 1α and tumor growth by inhibiting mitochondrial ROS production. Oncogene 30: 2986-2996, 2011.